Numerical simulation of capillary loop convective Polymerase chain reaction (clcPCR)

Author: [1]**Ping-Hei Chen,** [1]**Kamau Kingora.**

Presented to: NTU. Computer and information networking center

2017/03/31

Department of Mechanical Engineering, National Taiwan University, No. 1,Sec.4,Roosevelt Road.,Taipei,10617,Taiwan,R.O.C

Abstract

The current work intends to investigate the physics of natural convection in a tube. The properties of fluid is modeled to fit the properties of polymerase chain reaction reagents. The phenomena of natural convection with the tube heated from the bottom and the top open to the atmosphere will be simulated. The flow regimes and the temperature profiles will then be compared with the experimental results. 3-dimensional incompressible Navier-Stokes equation and the energy equation will be solved in Cartesian grid system. An in-house c++ code parallelized using openMP running on four processors on a shared memory is employed for this task. Simulation of two dimensional flow in a squire enclosure shows that the results obtained in the current study is in agreement with the already published results for moderate Rayleigh's number (Ra).

Keywords: Polymerase chain reaction , natural convection, ccPCR, Rayleigh's number

1. Introduction

Natural convection is one of the ways to enable rapid DNA amplification through the polymerase chain reaction (PCR). ccPCR is particularly attractive due to its simplicity. The traditional three temperature controls corresponding to the optimal temperature for enzymatic action involved in denaturing, annealing and extension are replaced by one temperature control. By the virtue of Rayleigh Bernard convection, the reagents pass through the various temperatures optimal for various enzymatic action.

Table 1: Temperature requirement for PCR

Temperature requirement for each of ccPCR steps		
step	Temperature ^{0}C	reaction time
Denaturing	90 - 96	instantaneous
annealing	55 - 60	instantaneous
extension	72 - 75	~40 bases per second

Careful design of ccPCR tube is necessary to optimize not only the temperature but also the time taken for each step of the amplification process. Trial and error method prohibitively costly since PCR reagents are very expensive. Numerical simulation is very handy in studying the optimal tube dimensions for a given Ra.

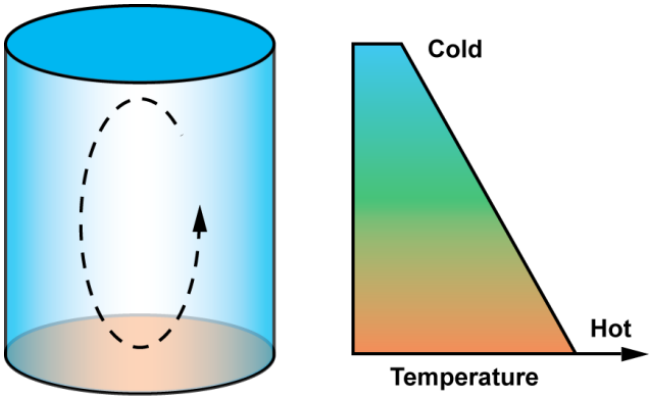

Figure 1: Schematic of Rayleigh Bernard convection in a cylinder. (Maddu .R .M . G (2010))

Owing to the geometry of a cylinder, the flow is 3 dimensional. In this study, 3-D incompressible Navier-Stokes equation and the energy equation will be solved by use of an in-house c++ code. The parameters to be studied include the aspect ratio of the cylinder, Ra and the shape of the container.

2. Solution method to Navier-Stokes equation.

Incompressible Navier-Stokes equations has been solved using finite volume scheme with staggered grid arrangement. Explicit energy equation has also been solved. Direct forcing immersed boundary method is employed to implement the no slip boundary conditions at the walls of a capillary tube.

2.1 Governing equations

The non-dimensional continuity, momentum and energy equations governing incompressible Newtonian fluid flow are expressed as follows:

C-E $$\nabla \cdot \mathbf{u}^* = 0$$

M-E $$\frac{\partial \mathbf{u}^*}{\partial t^*} + \nabla \cdot (\mathbf{u}^* \mathbf{u}^*) = -\nabla \cdot p^* + \sqrt{\frac{\Pr}{Ra}} \nabla^2 \mathbf{u}^* + \theta$$

E-E $$\frac{\partial \theta}{\partial t^*} + (\mathbf{u}^* \bullet \nabla)\theta = \frac{1}{\sqrt{\Pr\ Ra}} \nabla^2 \theta$$

Where $\mathbf{u}^*$ is the dimensionless velocity vector.

p^* is the dimensionless pressure.

Ra is the Rayleigh's number.

Pr is the Prandtl's number.

θ is the dimensionless temperature.

2.2 Numerical solution

In present study, implicit finite volume method discussed in Versteeg and Malalasekera (2007) is applied to solve the Navier-Stokes equations in Cartesian grids with staggered grid arrangement. The spatial and temporal discretization are done using the numerical schemes discussed below.

Spatial and temporal discretization

The diffusive and the convective terms of M.E are discretized using the second-order central difference scheme and the third-order quadratic upstream interpolation for convective kinetics (QUICK) scheme proposed by Leonard (1979), respectively. For the temporal terms, the Crank-Nicolson method is applied. This scheme can ensure second-order accuracy of temporal term discretization.

2.3 Mathematical formulae and numerical model

Prediction-correction for pressure-velocity

The velocity predicted by M.E may not be divergent free. To satisfy the continuity equation, SOLA algorithm is implemented. SOLA employs a gauss-seidel iteration to solve the pressure Poisson equation using inverse Poisson operator. A comprehensive procedure on the implementation of SOLA is given by Hirt et al (1975).

Procedures for complex shape no slip boundary condition

The complete numerical procedures for each time step of the proposed are summarized in the following algorithm.

1. Identify the immersed boundary location and determine the volume-of-solid function at each cell.

2. Compute the intermediate velocity by including the diffusive and convective terms.

3. Solve the pressure Poisson equation and correct the pressure and velocity field iteratively until the velocity is divergent free.

4. Solve the virtual force in the entire domain.

5. Update the velocity field using the calculated virtual force to implement the nonslip boundary condition

6. Solve the energy equation using the divergent free velocity to obtain the new temperature distribution.

7. Solve the virtual force for the energy equation using the new temperature distribution.

8. Update the temperature field using the virtual force obtained in step seven to enforce the thermal boundary condition.

2.4 Computational details and computing time

The computational domain of 1 ×1 ×1 is will be used.

At the end of the simulation, all the field variables in the computational domains are saved. A typical case requires about 30 GB of hard disk space. In a normal scenario, about 12 of such cases need to run at any simultaneously hence about 500GB of memory is required. The results presented in this report were obtained by using a cluster machine with 48 processors running on a shared memory. Due to the confidentiality of the data, only the data at the center z-plane will be presented in most of the cases. Intel c++ compiler (icc or icpc) with OpenMP (-fopenmp) library is used to compile the in-house code. Alternatively, g++ compiler can be used. Each case runs on at least 4 processors on a shared memory. No parallelization in a distributed memory is necessary.

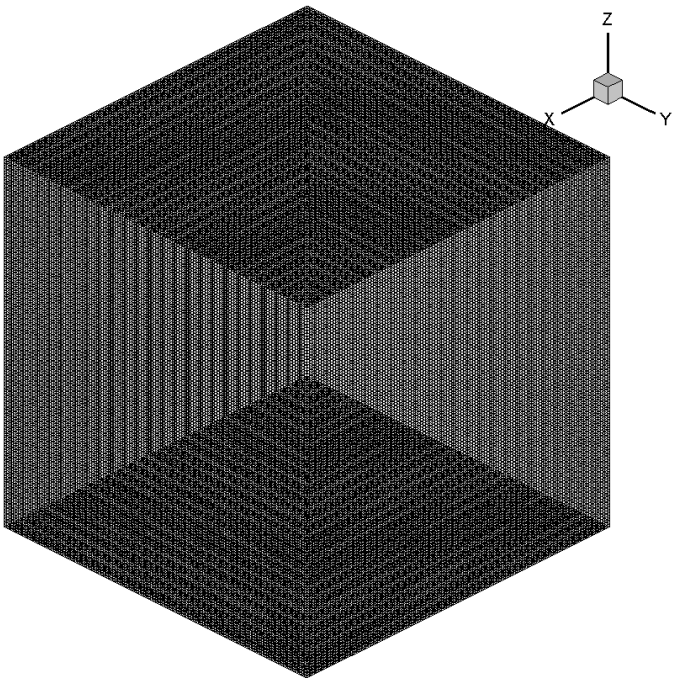

Figure 2: 3D mesh for simulation of natural convection in a cubical enclosure.

A non-uniform mesh with grids clustered in the vicinity of a solid wall and phase transition region is utilized. Grid stretching is accomplished by geometric progression. The mesh consists of 4×10^6 calculation points, the mass convergence criterion at each time step is set as 10^{-4}. OpenMP is used to achieve parallel computing between four processors sitting on a uniform access memory.

The longest simulation takes about 28 days to reach steady state at a PC cluster consisting of Intel Xeon E31220 processors 3.10 GHz.

2.5 Boundary conditions

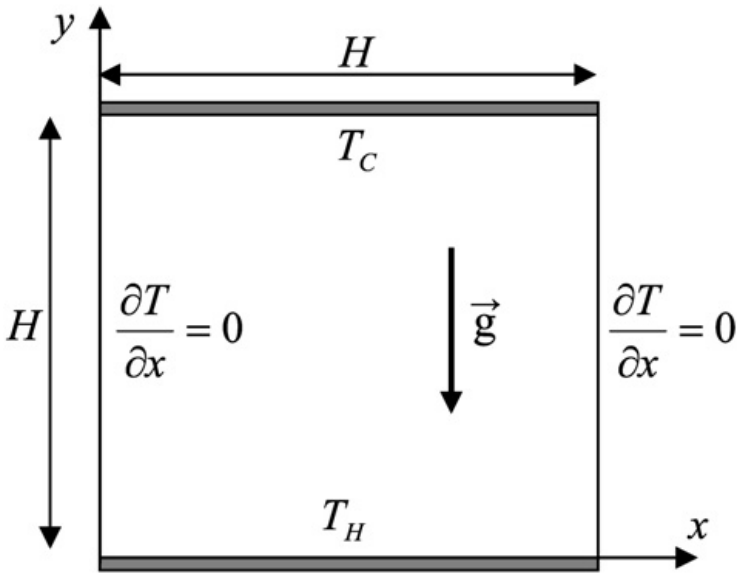

Figure 3: 2D representation of the boundary condition for natural convection in a cubical enclosure with differentially heated walls.

3. Results and discussion

2D natural convection in a squire cavity has been simulated. The left and the right wall were insulated while the bottom and the top walls were maintained at 0^0 C and 1^0 C respectively. No slip boundary condition was prescribed at all the walls. The working fluid for this simulation is air with Pr = 0.71.

3.1 Flow visualization (Velocity profile)

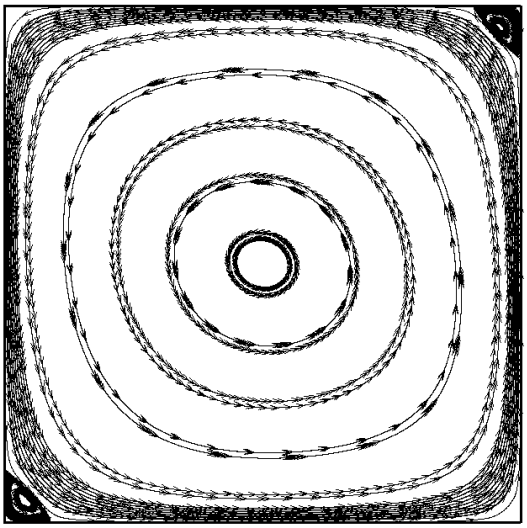

Figure 4: Streamlines of 2-D simulation of natural convection in a squire enclosure at Ra = 10^4.

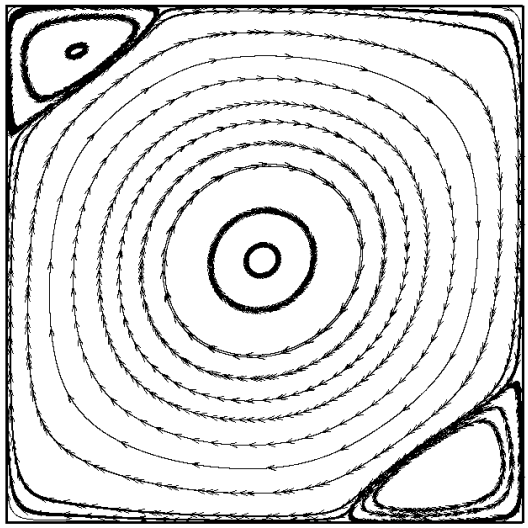

Figure 5: Streamlines of 2-D simulation of natural convection in a squire enclosure at Ra = 10^5.

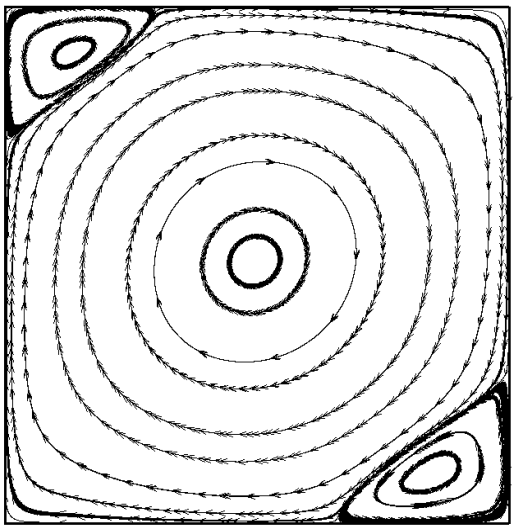

Figure 6: Streamlines of 2-D simulation of natural convection in a squire enclosure at Ra = 10^6.

Figure 7: Streamlines of 3-D simulation of natural convection in a cubical enclosure at Ra = 10^5.

The main circulation vortex is seen at the center of the cavity and secondary vortices are seen at the corner of the cavity. As the Ra increases, the circulation at the corners of the cavity enlarges. This feature is a little difficult to plot in three dimensional space.

3.2 Temperature profile

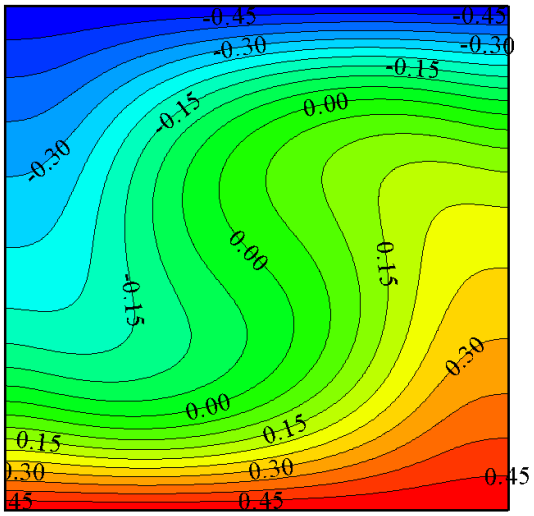

Figure 8: Temperature profile of 2-D simulation of natural convection in a squire enclosure at Ra = 10^4.

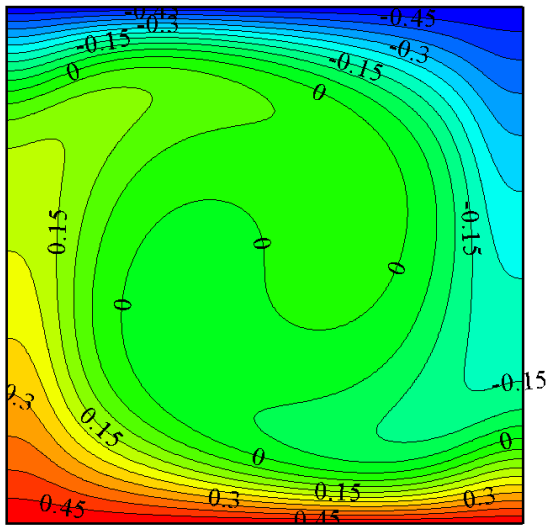

Figure 9: Temperature profile of 2-D simulation of natural convection in a squire enclosure at Ra = 10^5.

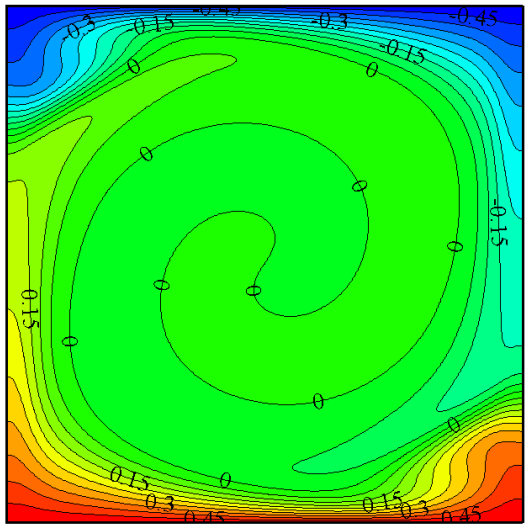

Figure 10: Temperature profile of 2-D simulation of natural convection in a squire enclosure at Ra = 10^6.

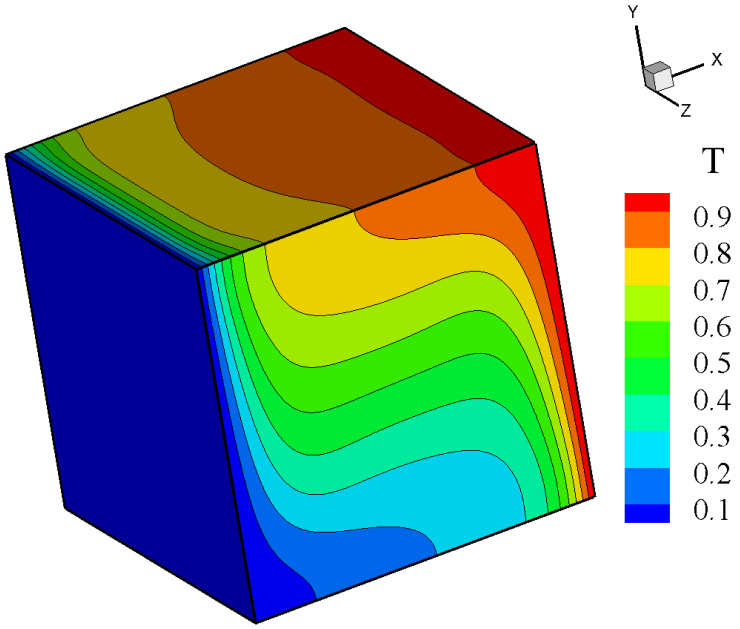

Figure 13: Temperature contours at the surface for 3D simulation at Ra = 10^5

Figure 11: Temperature profile of 3-D simulation of natural convection in a squire enclosure at Ra = 10^5.

3.4 3D Temperature distribution

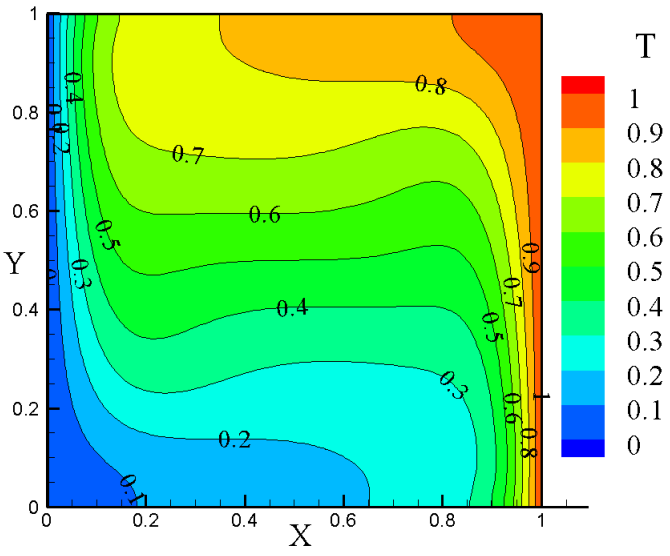

Figure 12: Temperature profile at z-mid plane for 3D simulation at Ra = 10^5

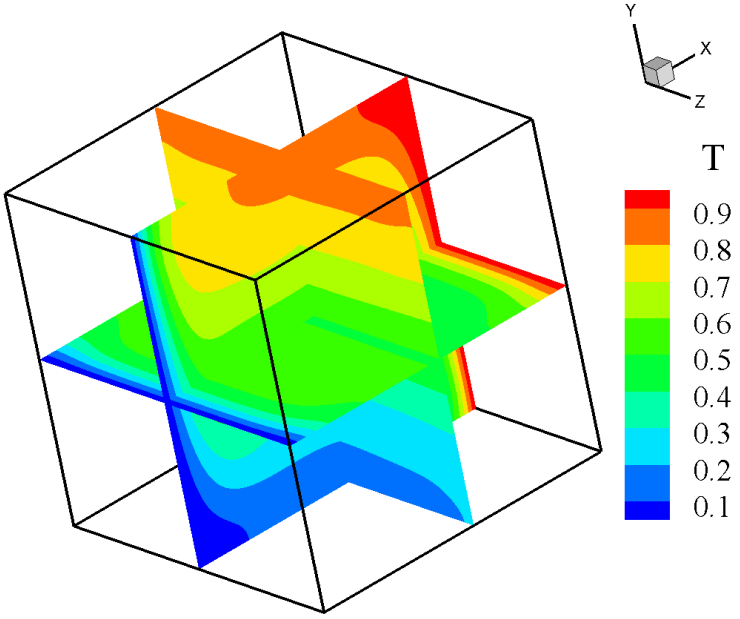

Figure 14 Temperature profile at mid planes for 3D simulation at Ra = 10^5

3.4 3D Velocity profiles

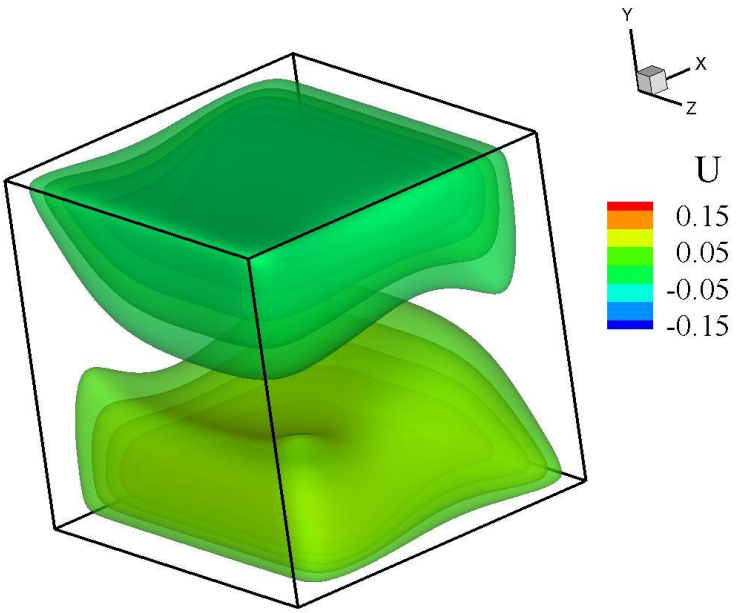

Figure 15: Velocity U isosurface at Ra = 10^5

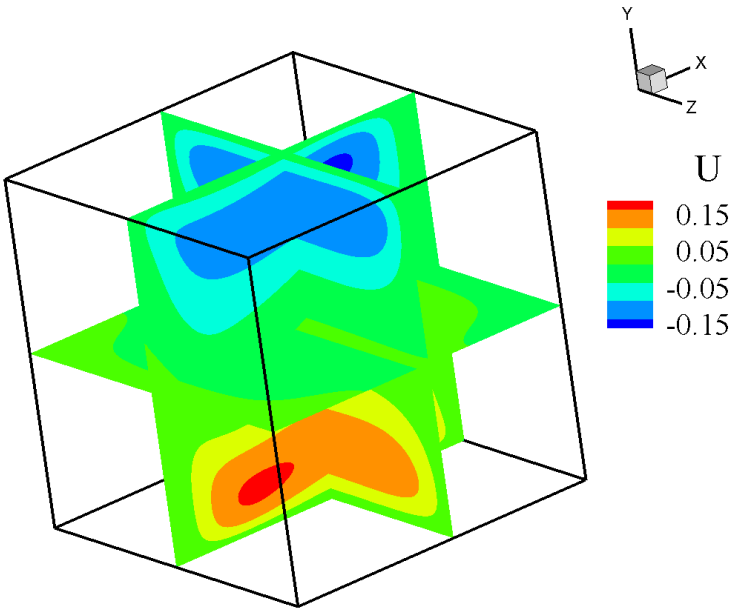

Figure 16 : Magnitude of Velocity U at mid planes at Ra = 10^5

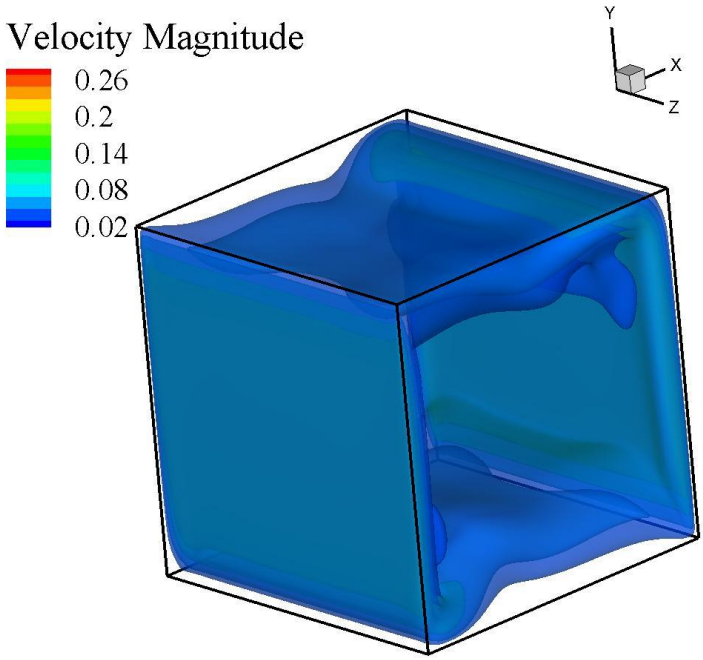

Figure 17: Isosurfaces of velocity vector magnitude

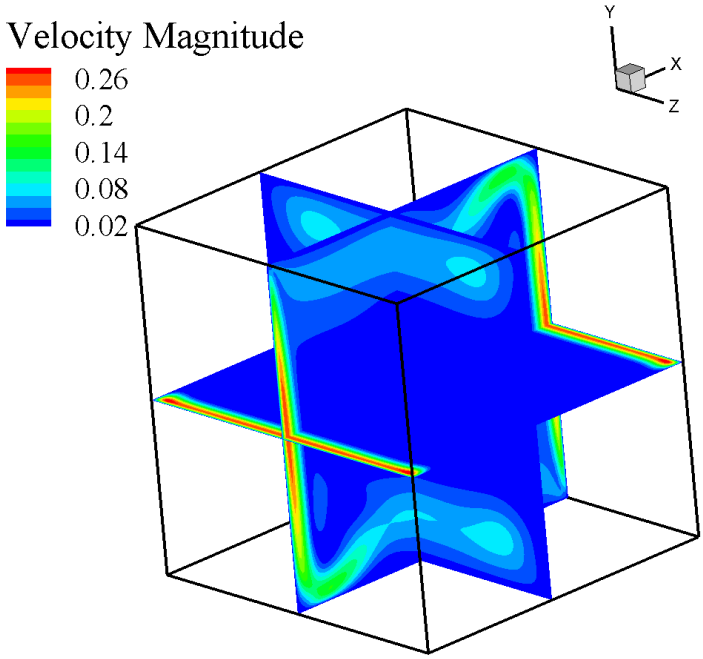

Figure 18 : Magnitude of Velocity at mid planes at Ra = 10^5

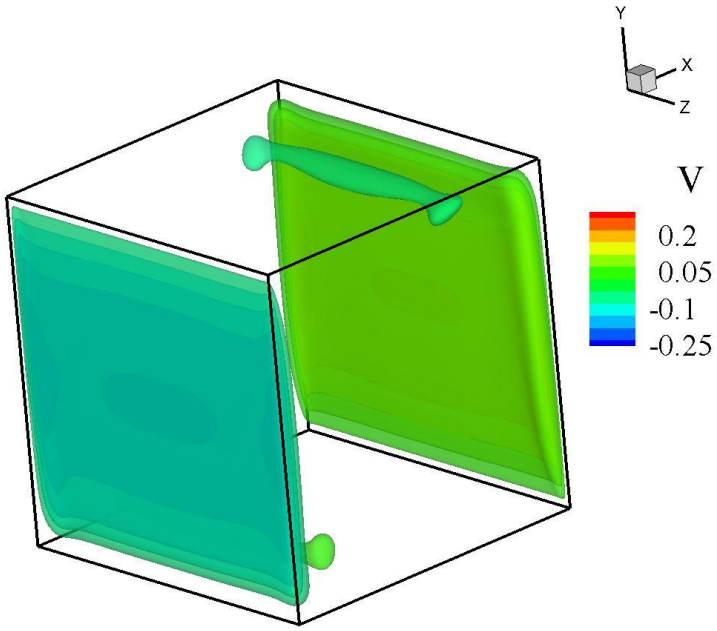

Figure 19: Velocity U isosurface at Ra = 10^5

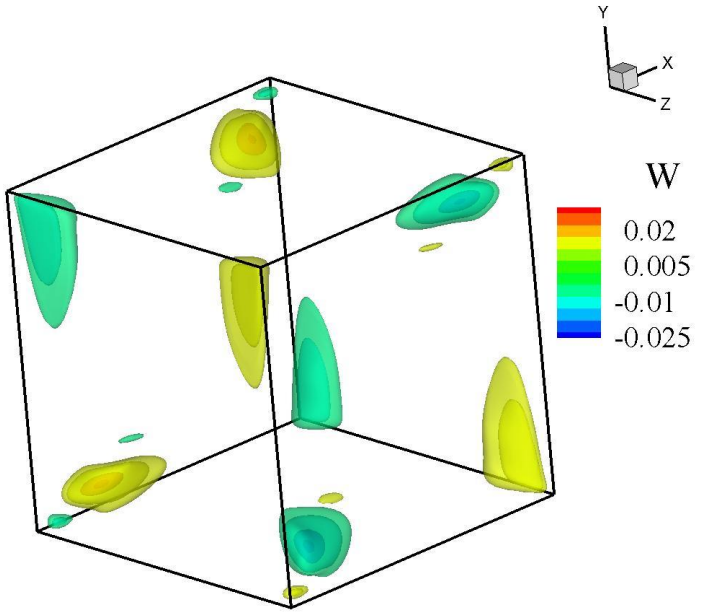

Figure 21: Velocity W isosurface at Ra = 10^5

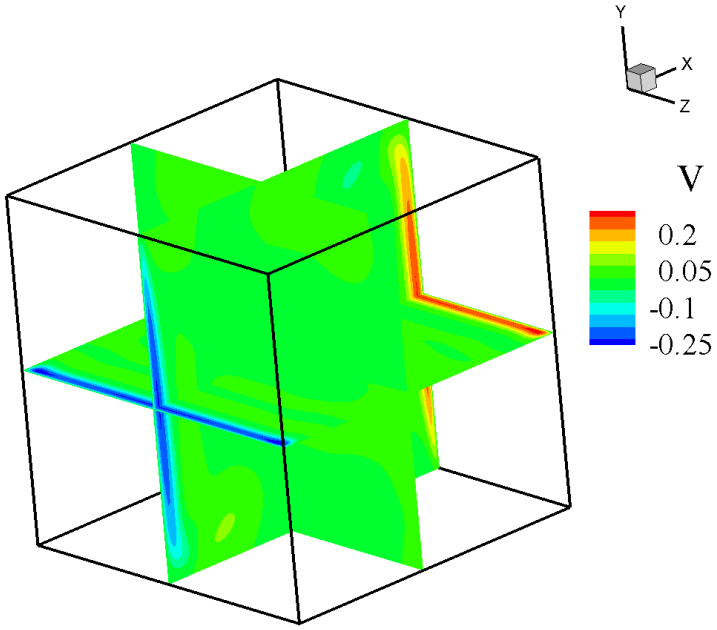

Figure 20: Magnitude of Velocity V at mid planes at Ra = 10^5

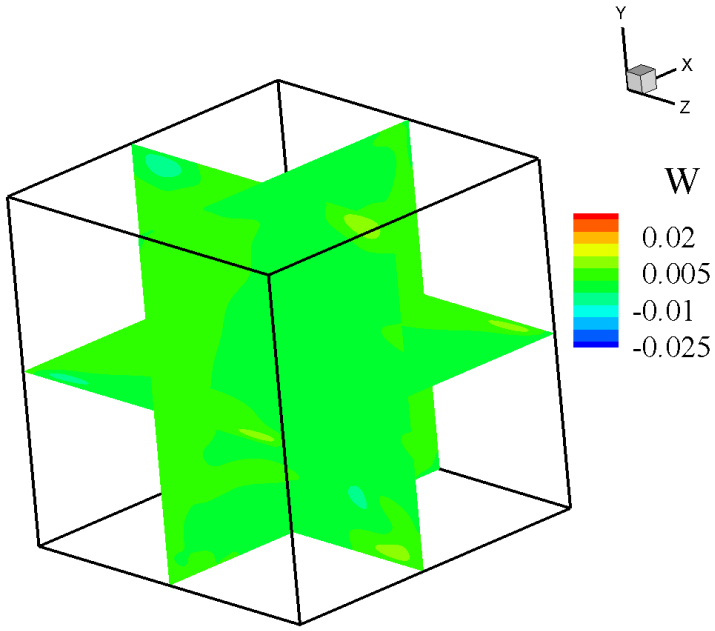

Figure 22: Magnitude of Velocity W at mid planes at Ra = 10^5

3.4 3D Vorticity profiles

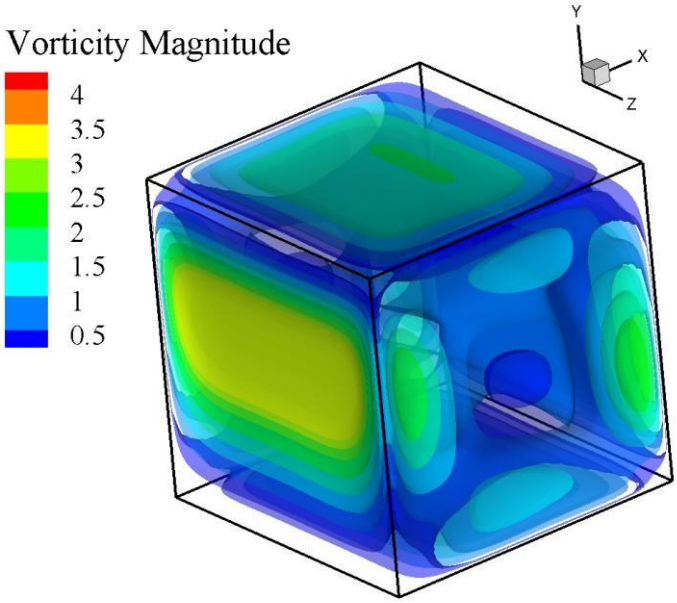

Figure 23: Isosurfaces of vorticity magnitude at Ra = 10^5

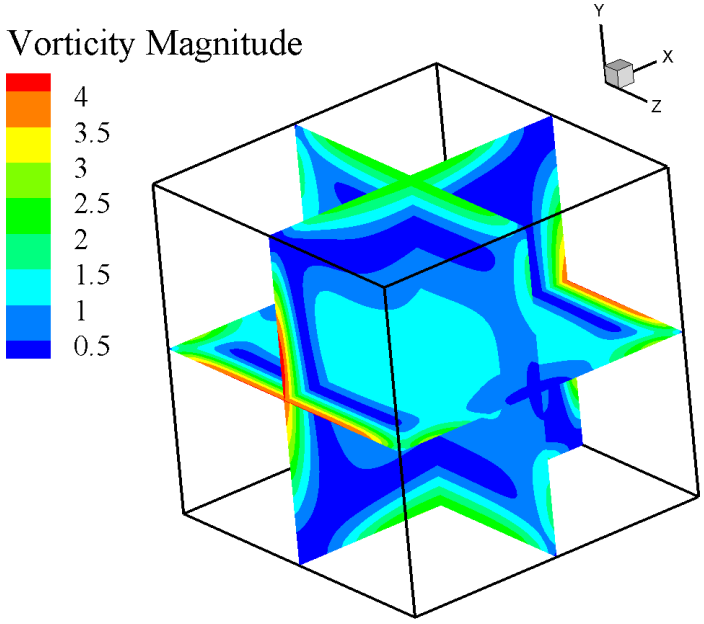

Figure 24: Magnitude of vorticity at mid planes at Ra = 10^5

3.5 3D local Nusselts number distribution at the hot wall

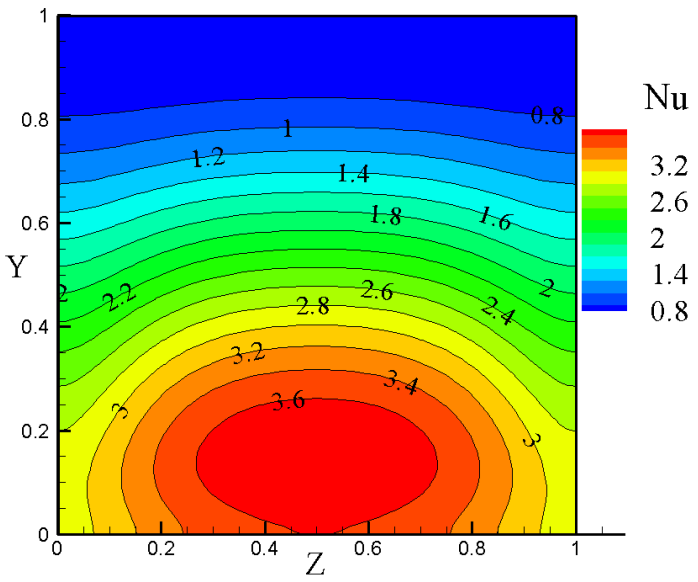

Figure 25: Local Nusselts number distribution at the hot wall for Ra = 10^4

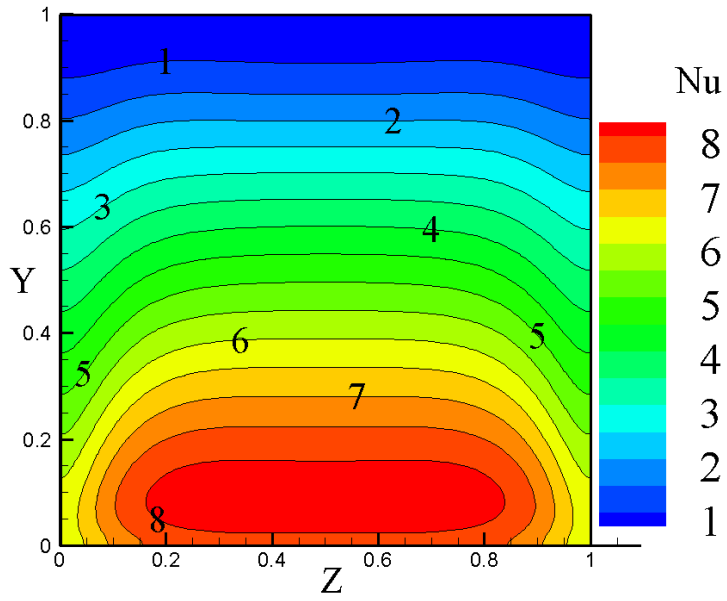

Figure 26: Local Nusselts number distribution at the hot wall for Ra = 10^5

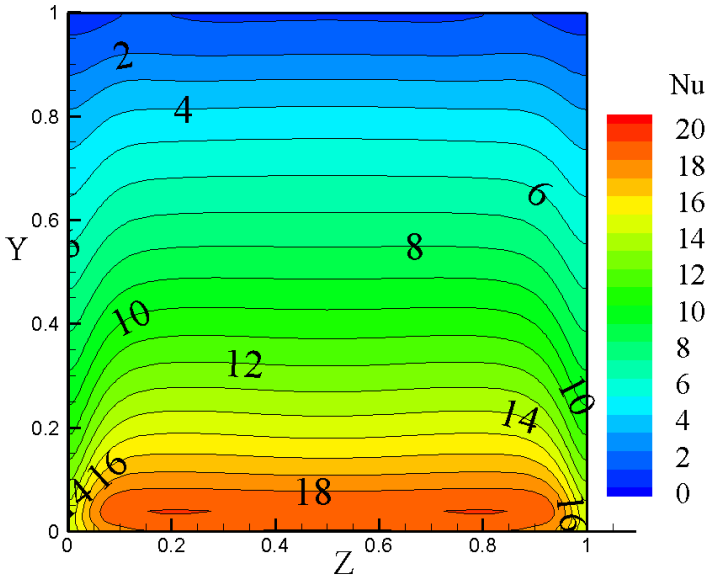

Figure 27: Local Nusselts number distribution at the hot wall for Ra = 10^6

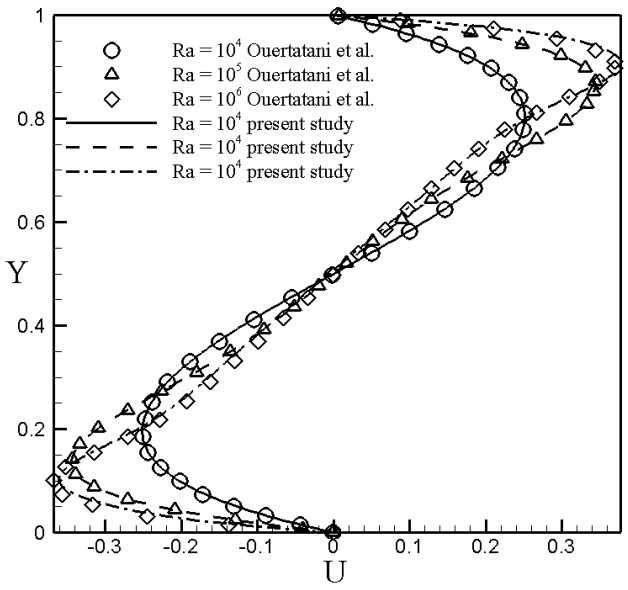

Figure 29: The velocity profile of U-velocity along the vertical centerline for 2D simulation at various Ra.

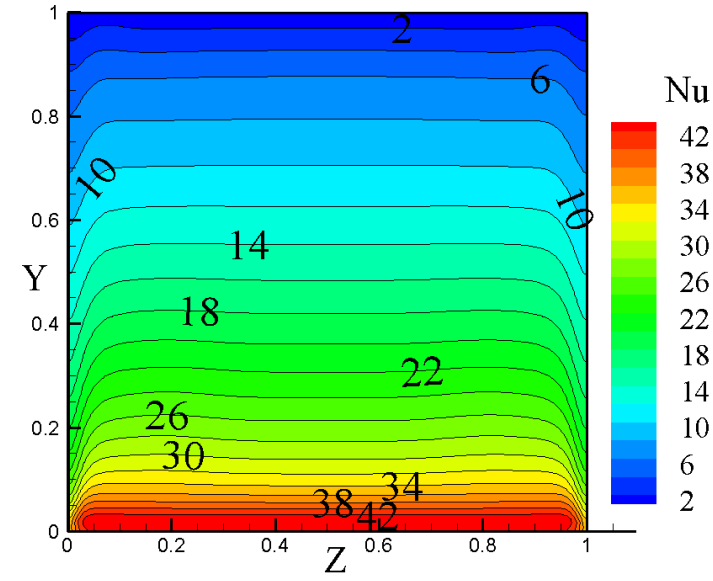

Figure 28: Local Nusselts number distribution at the hot wall for Ra = 10^7

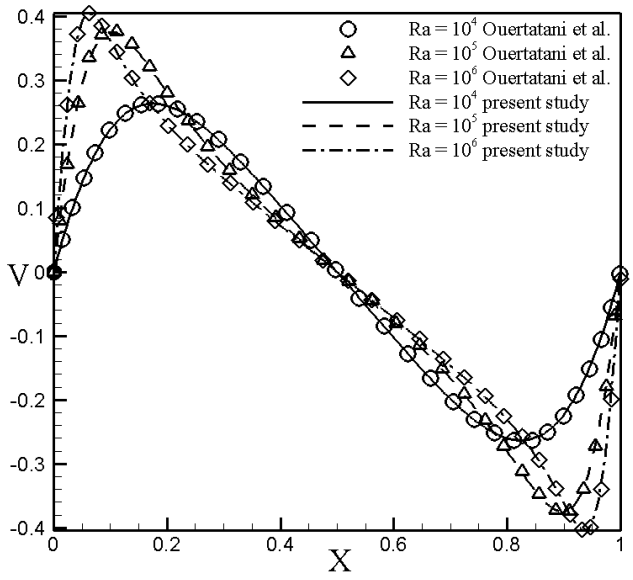

Figure 30: The velocity profile of V-velocity along the horizontal centerline for 2D simulation at various Ra.

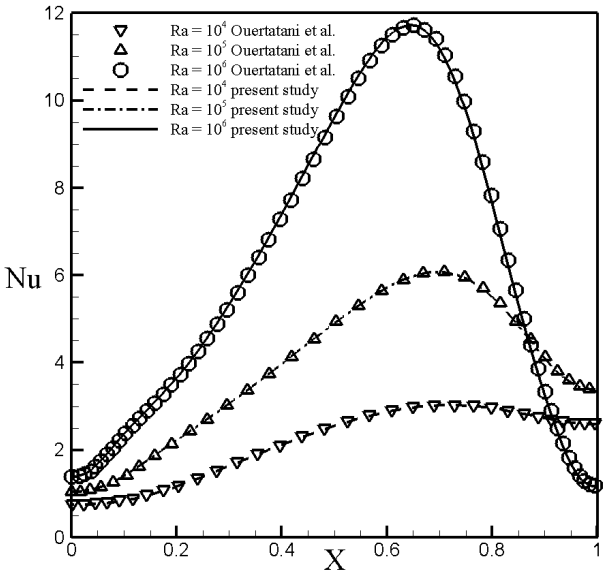

Figure 31: The local Nu profile along the bottom wall for 2D simulation at various Ra.

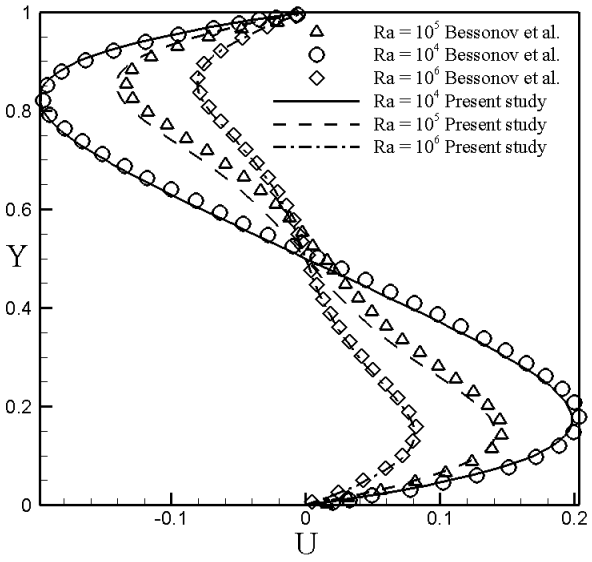

Figure 33: The velocity profile of U-velocity along the vertical centerline for 3D simulation at various Ra.

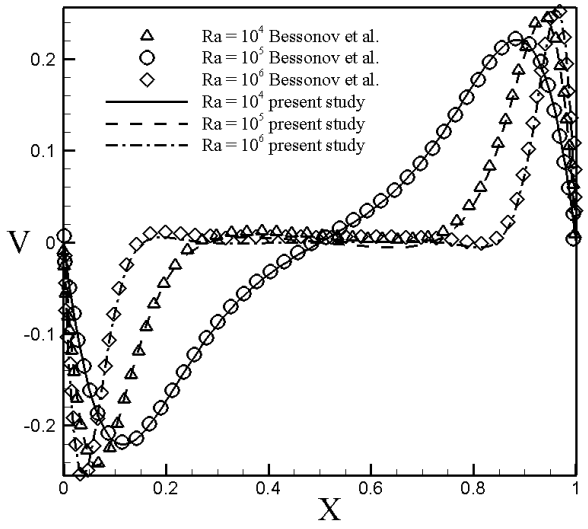

Figure 32: The velocity profile of V-velocity along the horizontal centerline for 3D simulation at various Ra.

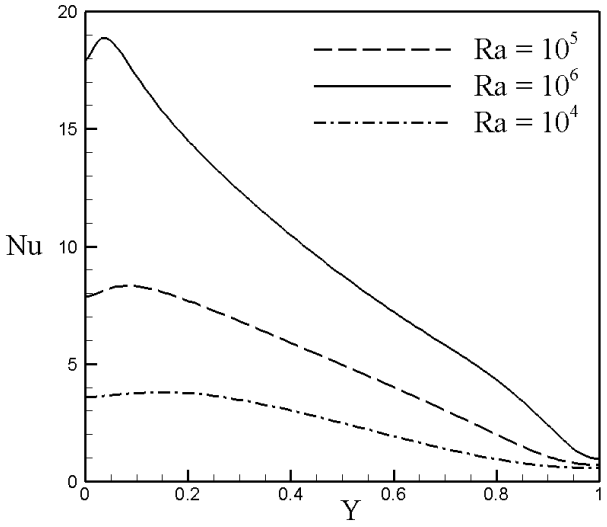

Figure 34: Distribution of local Nu at the centerline of hot wall for x=1, z=0.5.

Table 2: Comparison of coordinate position for u_{max} and v_{max} between the present study and the published results.

Ra	Researcher	y(u_{max})	x(v_{max})
10^4	Ouertatani et al.	0.8023	0.8263
	Present study	0.8203	0.8359
10^5	Ouertatani et al.	0.8636	0.8973
	Present study	0.8750	0.9063
10^6	Ouertatani et al.	0.9036	0.9359
	Present study	0.9104	0.9297

4.0 Numerical simulation of clcPCR

Natural convection in a clcPCR tube was reported by Chou et al. (2017). Their design (Fig.) was fabricated out of glass and tests were carried out in a lab environment of still air at 23^0C.
Fig. 20 shows the domain and boundary conditions of a typical clcPCR tube. The heat loss through side walls is modeled to mimic convective boundary conditions taking into account thermal
resistance of glass tube. Initially, the fluid is at rest, $u_0 = v_0 = w_0 =$

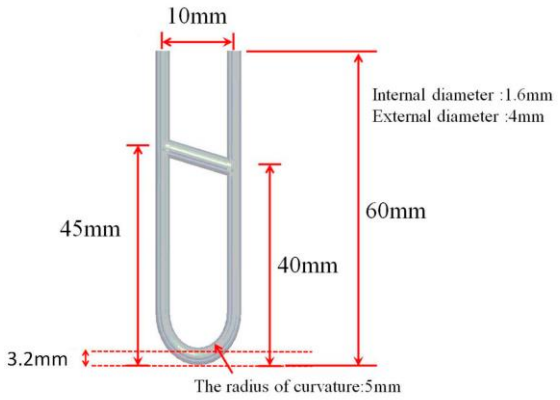

0.

Figure 35. Design of clcPCR tube as proposed by Chou et al. (2017)

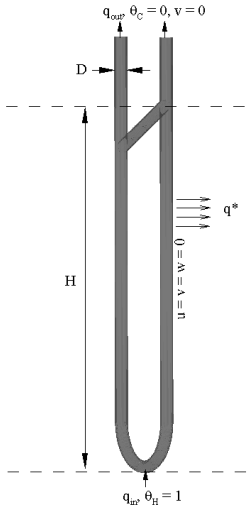

Figure 36. Domain and boundary conditions for simulation in a U-tube

Flow visualization

When heating starts, the uid is at rest.
As more heat is added, the uid becomes unstable and two vortices start to form as shown in Fig.
21 (a). These vortices grow as more heat is added initiating ow around the tube (Fig. 21 (b)
and (c)). As more heat is added, ow around the tube increases as initial vortices decrease before
disappearing altogether (Fig. 21 (d) and (e)). Finally, Circulation starts at the tubes _rst junction
visited by the uid. This ow patters persists until steady state.

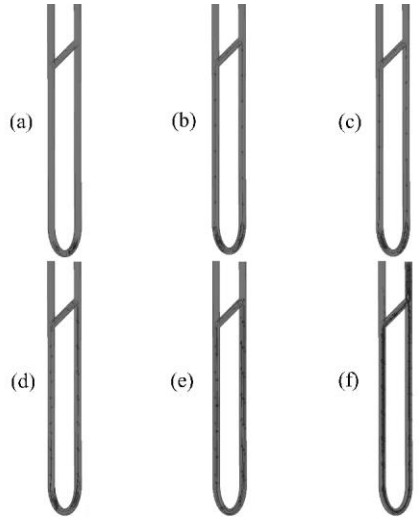

Figure 17. Flow visualisation for natural convection in a clcPCR tube at (a) 5 s (b) 10s (c) 20s (d) 30s (e) 40s (f) 80s

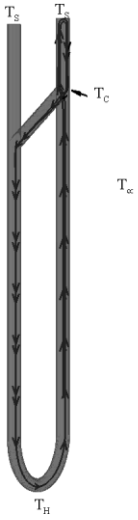

Figure 38. steady state Flow visualisation for simulation of natural convection in a clcPCR tube

Temperature Distribution

The temperature distribution in a clcPCR tube is affected by a number of variables including the
environment temperature T∞ and the area of free surface. In the current simulation, T∞ = 23^0C and H / D= 28 corresponding to experiment of Chou et al. (2017). 104W of heat was added to the tube's base to yield a temperature of 90^0C at the base. 47% and 53% of heat input was lostthrough glass wall and free surface, respectively. Temperature pro_le predicted by the current natural convection model is presented in the figure below..

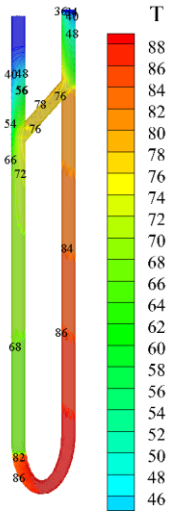

Figure 2Temperature distributuion for natural convection simulation in a clcPCR

Velocity profile

The figure below presents a plot of dimensionless velocity vertical component, v, along the x-centerline (Y = 0.5H, Z = 0.5D). The velocity profile is parabolic insinuating laminar ow in clcPCR tube with
v_{max} = 0.084. By integrating velocity along streamlines, average time taken in a single circulation around the clcPCR tube was determined as 12.46s.

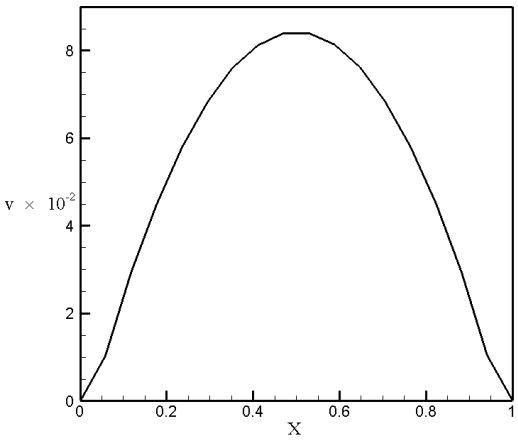

Figure 3 Plot of v velocity component along the x-centerline (y = 0:5; z = 0:5)

Conclusion

3D Navier-Stokes equation has been solved using an implicit finite volume discretization scheme. The diffusion term is solved using 2nd order central differencing scheme and the convective term is solved using 3rd order QUICK scheme. The temporal term is solved using Crank - Nicolson method ensuring at least 2nd order accuracy in time discretization. Pressure velocity iteration are carried out using SOLA algorithm. The energy equation is solved using explicit finite volume discretization.

Comparison between flow visualization in the present simulation and the published results shows that the pattern of flow obtained presently is consistent with the published data. For 2D simulation, the value of mean Nu is found to be 2.158, 3.9157 and 6.3086 for Ra = 10^4, 10^5 and 10^6 respectively. In 3D simulation, the values of the mean Nu are found to be 2.0609, 4.3496 and 8.7281 for Ra 10^4,105 and 10^6 respectively. These results are in good agreement with the published results i.e. within 0.1% error margin.

The velocity profile at the centerline plotted for various Ra. Coordinate of maximum velocity as well as the value for the maximum velocity are also compared with the published solution. Form the results, it is evident that the physics of natural convection is solved accurately enough using the current scheme.

Similar rigorous simulation need to be done for free convection in the tube. Due to the complexity of the shapes, e.g. U-tube, high mesh resolution is required as compared to the present resolution. The parameters of interest include the effect of the aspect ratio of the capillary tube as well as the time taken to achieve the first circulation. Owing to the current results, the researchers are optimistic that the current in-house numerical code can solve the above problem accurately.

References

1. Noor, D.Z., Chern, M.J., Horng, T.L., 2009. An immersed boundary method to solve fluid-solid interaction problems. *Computational Mechanics* **44**, 447–453.
2. Leonard, B.P., 1979. A stable and accurate convective modelling procedure based on quadratic upstream interpolation. *Computer Methods in Applied Mechanics and Engineering* **19**, 59–98.
3. Hirt, C.W., Nichols, B.D., Romero, N.C., 1975. A numerical solution algorithm for transient fluid flows. Technical Report AD-A009953, Los Alamos Scientific Laboratory,USA .
4. Versteeg, H.K., Malalasekera, W., 2007. *An Introduction to Computational Fluid Dynamics*. 2nd ed., Pearson Education Limited, U.K.
5. Radha Malini Gowri Muddu, 2010. *Three Dimensional Simulation Of Rayleigh-Bénard Convection For Rapid Microscale Polymerase Chain Reaction*. Ph.D. Thesis, Texas University. U.S.A.
6. Bessoov, O.A., Brailovskaya, V.A., Nikitin, S.A., Polezhaev, V.I., 1997. Three-dimensional natural convection in a cubical enclosure: A bench mark numerical solution. *International Centre for Heat and Mass Transfer* **160**, 9 pages.
7. Chou, W. P., Lee. C., Hsu, J. Z., Lai, M. H., Kuo, L. S. Chen, P. H., 2017. Development of capillary loop convective polymerase chain reaction platform with real-time fluorescence detection.. *Inventions* **2**, 2010003.
8. Ouertatani, N., Cheikh, B.N., Beya, B.B., 2007. Numerical simulation of two- dimensional Rayleigh–Bénard convection in an enclosure. *Comptes Rendus Mécanique* **336**, 464–470.